Eur. Phys. J. D (2023)77:125
https://doi.org/10.1140/epjd/s10053-023-00698-2

THE EUROPEAN PHYSICAL JOURNAL D

Regular Article – Atomic and Molecular Collisions

High-resolution X-ray emission study for Xe^{54+} on Xe collisions

Marc Oliver Herdrich[1,2,3,a], Daniel Hengstler[4], Michael Keller[4], Jeschua Geist[4], Christian Schötz[4], Matthäus Krantz[4], Andreas Fleischmann[4], Christian Enss[4], Tobias Gassner[1], Pierre-Michel Hillenbrand[1,5], Alexandre Gumberidze[1], Uwe Spillmann[1], Sergiy Trotsenko[1], Paul Indelicato[6], and Thomas Stöhlker[1,2,3]

[1] GSI Helmholtz Center for Heavy Ion Research, Planckstraße 1, 64291 Darmstadt, Hesse, Germany
[2] Helmholtz-Institute Jena, Fröbelstieg 3, 07743 Jena, Thuringia, Germany
[3] Institute for Optics and Quantum Electronics, Friedrich-Schiller-University Jena, Max-Wien-Platz 1, 07743 Jena, Thuringia, Germany
[4] Kirchhoff-Institute for Physics, Ruprecht Karls University Heidelberg, Im Neuenheimer Feld 227, 69120 Heidelberg, Baden-Württemberg, Germany
[5] Institute of Experimental Physics I, Justus-Liebig-University Giessen, Heinrich-Buff-Ring 16, 35392 Giessen, Hesse, Germany
[6] Laboratoire Kastler Brossel, Sorbonne Université, CNRS, ENS-PSL Research University, 24 Rue Lhomond, 75005 Paris, France

Received 25 April 2023 / Accepted 7 June 2023

Abstract. We report on an experiment conducted at the ESR storage ring aiming at the study of the X-ray emission of Xe^{54+} ions colliding with Xe atoms at a beam energy of 50 MeV/u. The radiation resulting from the ion–atom interaction was observed using a high-resolution spectrometer based on metallic–magnetic calorimeter technology. In order to benchmark the capabilities of these detectors for high-precision atomic physics experiments, we identified several transitions from H-like and He-like xenon and determined their energies. Furthermore, the 1*s*-Lamb shift in Xe^{53+} was estimated using the measured line energies. The results are compared with previous experimental studies and theoretical predictions.

1 Introduction

X-ray spectroscopy experiments involving highly charged heavy ions have become an indispensable tool for tests of quantum electrodynamic (QED) effects in strong fields [1]. In the past, measurements with H-like and He-like Xe ions have been performed by several groups at different experiment facilities (see, for example, [2–4]). In this work, we present the results of an experiment that was conducted at the *ESR* ion storage ring of GSI [5] utilizing a cryogenic calorimeter detector for high-precision X-ray spectroscopy. Metallic–magnetic calorimeters (MMC) like the maXs-series detectors developed in cooperation with the Kirchhoff-Institute for Physics (KIP) in Heidelberg [6–8] combine several advantages over conventional energy-dispersive X-ray photon detectors. They can reach resolving powers of $E/\Delta E > 6000$ [9]–comparable to crystal spectrometers–over a broad spectral acceptance range–comparable to typical semiconductor detectors. Together with an excellent linearity [10] as well as signal rise times up to $\tau_0 \approx 100\,\text{ns}$ [11] they are particularly well suited for high-precision X-ray studies in atomic and fundamental physics experiments dealing with heavy, highly charged ions. However, in order to achieve this extraordinary performance, a transition from conventional analog to fully digital data processing and analysis is required. Therefore, a software framework for analyzing MMC data has been developed during the course of several experiments conducted at the ion storage facilities of GSI/FAIR in the last years. In the following, the experiment and the MMC detector are briefly described in Sects. 2 and 2.1, respectively. The detailed analysis of the recorded data in Sect. 3 is followed by a short conclusion about the feasibility of using cryogenic microcalorimeter detectors in the context of precision spectroscopy related to fundamental tests of the standard model (see Sect. 4).

2 Experiment

The experiment is described in detail in [12,13]. It involved an electron-cooled $^{132}Xe^{54+}$ ion beam at 50 MeV/u beam energy colliding with a Xe gas-jet at the internal target of the ESR ion storage ring. In order to record X-ray photons resulting from the ion–atom inter-

[a] e-mail: m.o.herdrich@hi-jena.gsi.de (corresponding author)

Published online: 01 July 2023

action, a maXs-200 detector [7] was positioned in front of the 60° port of the target chamber. The pixels of this 1×8 spectrometer array consist of a gold absorber and a Au:Er-based paramagnetic sensor in a gradiometric configuration with two pixels connected to a SQUID-based readout and amplification stage. It was mounted with its pixels in vertical orientation (to reduce Doppler broadening) at the tip of the 60 cm long cold finger of a ^{3}He/^{4}He dilution cryostat in order to achieve the required operation temperature of < 30 mK. The nominal absorption efficiency at 100 keV is 45% with an active detection area of 1 mm^2 per pixel. From previous testing of an identical detector chip, an energy resolution of 62 eV full width at half maximum (FWHM) at 60 keV was reported. The distance between the detector and the interaction point amounted to 2 m resulting in a 2.5×10^{-7}sr solid angle per pixel. A vacuum window made of diamond was installed on the target chamber, and the X-ray entry window in front of the MMC was made of aluminum-coated Mylar foils as well as a beryllium window for the separation of the surrounding vacuum from air. During the 48 h of almost continuous recording of X-ray radiation at the ESR, a ^{241}Am source was positioned in front of the detector (offset from the view port into the target chamber) for simultaneous calibration.

We note that an experiment with a similar setup was performed very recently [14]; however, only conventional photon detectors were used. Furthermore, a comparable experiment at even lower collision energies was conducted [15] utilizing a maXs-30 type detector. Though, too few events were detected by the microcalorimeter at that time to perform a proper analysis.

2.1 Detector performance

The absolute energy calibration of the detector was performed by fitting a gaussian distribution to the peaks of the well-known lines of the ^{241}Am calibration source for each pixel individually. The central positions of the peaks were then compared to the corresponding energies reported in the literature. A fit using a second-order polynomial thereby takes into account the well understood nonlinearities of the detector. Additionally, unavoidable temperature fluctuations of the detector's substrate during the measurement lead to a spectral broadening due to a linear temperature dependance of the sensor's gain behavior. This effect could be mostly compensated by using the baseline level (before the trigger) of each recorded signal as its temperature information. Comparing the measured energies of events associated with the 59.5 keV calibration line to their corresponding sensor temperatures allowed for the calculation of a regression line which was then applied inversely to the rest of the events. An in-depth description of all utilized calibration and correction procedures can be found in [8].

The instrumental energy resolution determined from the line width of the observed calibration line at 26.3 keV
is found to be 42.0 eV (FWHM). However, from the characterization of the baseline noise one finds an expected resolution of 38.2 eV [12]. This can be partially explained by a loss of resolution power due to a remaining fraction of uncorrected temperature-dependent gain drift and signal shape (see [16]) artifacts. The line width of the measured X-ray lines from the ion–atom interaction amounts to 77 eV at around 35 keV. This difference to the calibration lines can be partially attributed to the finite size of the gas-jet target resulting in Doppler broadening, but has not been fully understood, yet [8]. Systematic uncertainties from the Doppler broadening between pixels are approximated to be below 4 eV [8]. Additional uncertainties due to calibration errors are also small compared to the overall resolution (approximated mean deviation from literature values are in the order of 1 eV). Therefore, both effects are ignored in the following analysis. During the experiment only two of the eight pixels were connected, therefore limiting the total amount of events available for the analysis.

3 Experimental data and results

Because of the comparably slow collision of 50 MeV/u and the symmetrical and heavy systems chosen (Xe^{54+} on Xe), one can assume an adiabatic exchange of one or more electrons between the fully ionized projectile ions and neutral target atoms [22]. The entire recorded spectrum can be seen in Fig. 1. The most prominent features stem from K-shell transitions (see also Fig. 2) within both collision partners, while L-shell transitions are not observable due to photon absorption in the diamond window and gap filled with air between target and detector. A first evaluation of the measured spectra can be found in [8,23].

3.1 Target radiation

At 30 keV, a group of transitions is visible that can be attributed to radiation emitted by the target atoms. It results from subsequent relaxation of excited states into electron vacancies produced by electron transfer from the target into the projectile ions. Observed are K-α transitions from different charge states of xenon with multiple satellite features caused by screening effects. A detailed analysis of this phenomenon is found in [14]. A comparison of energy limits for neutral down to H-like xenon ranges from Xe I K-α_2: 29,458.3 eV [24] to Ly-α_1: 31,283.9 eV [17]. This matches the recorded spectral features and indicates that in such collisions potentially a multitude of electrons can be stripped from the target atoms.

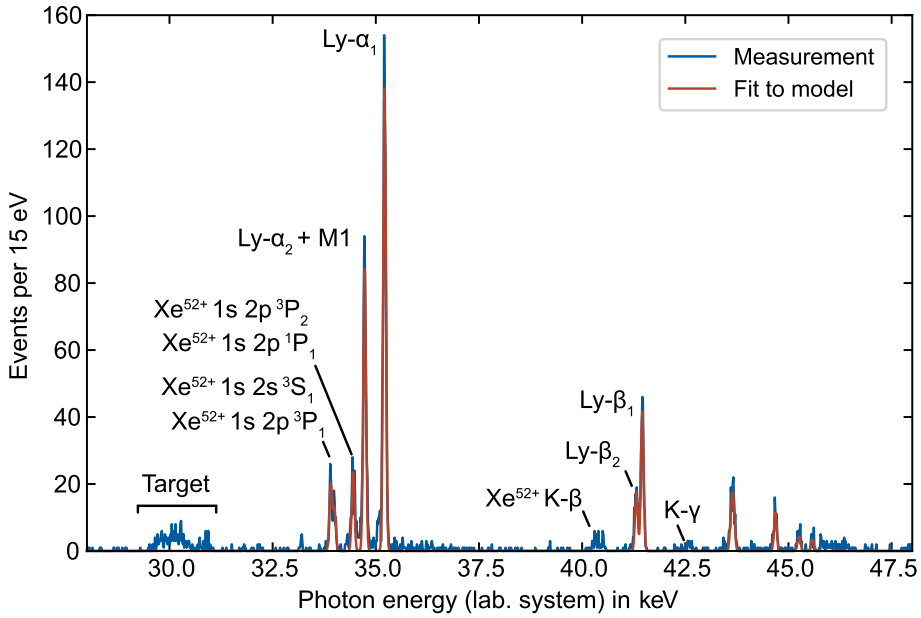

Fig. 1 Shown is the full spectrum recorded with a maXs-200 detector during the presented beam time. It contains X-ray events (from both pixels combined) from collisions between Xe^{54+} at 50 MeV/u and a Xe gas-jet target (blue curve). In red, the fitted model function containing the annotated transitions is overlaid. A preliminary version of the spectrum can be found in [12]

3.2 Projectile radiation

Electrons transferred into excited states of the projectile ions through non-radiative electron capture (NRC) [25] also lead to the emission of characteristic X-ray radiation via subsequent cascades. As can be seen in Fig. 1, the projectile radiation is significantly more intense than the radiation from the target. This can be explained by the fact that the NRC process (involving electrons from all target shells) has a much larger cross section for this collision system than the target K-shell vacancy production including electron transfer and direct Coulomb ionization responsible for the target X-rays.

3.2.1 Doppler correction and comparison to theoretical predictions

Observed K-shell transitions are shifted to higher energies compared to the target radiation due to a Doppler shift at the used observation angle resulting from the relativistically moving projectiles:

$$E = E^{'} \cdot f = E^{'} \cdot \gamma \left(1 - \beta \cos \theta^{'}\right) \tag{1}$$

With a beam energy of $E_{\mathrm{kin}} = 50.43 \pm 0.09\,\mathrm{MeV/u}$ (calculated from the applied electron cooler voltage of $27.70 \pm 0.05\,\mathrm{kV}$ at an electron beam current of 100 mA) and an observation angle of $\theta = 60 \pm 1^{\circ}$ a Doppler shift of $f = 1.1269 \pm 0.0064$ is expected. A model of superposed normal distributed peaks for all identified transition lines is fitted to the spectrum to extract the measured line positions. The most prominent K-α- and K-β-transition energies E^{*} from hydrogen-like xenon (see Table 1 and Fig. 3) are then used to perform a linear fit against the binding energies E_{i}—assumed to be known from our theoretical predictions [17]—of the participating excited states:

$$E^{*} = f \cdot (E_{\mathrm{i}} - E_{\mathrm{f}}) \tag{2}$$

This not only yields a more precise value for the actual Doppler shift but also allows to estimate the common ground state binding energy $E_{\mathrm{f}} = 41{,}299.93 \pm 2.78\,\mathrm{eV}$ (uncertainty taken from the fit). The resulting Doppler correction factor of $f = 1.125534 \pm 9.8 \times 10^{-5}$ is in good agreement with the expectation. Assuming that the beam energy is well known, this yields a corrected observation angle of $60.21 \pm 0.03^{\circ}$. At a distance of 2 m this gives rise to a difference of $7.39 \pm 0.92\,\mathrm{mm}$ to the assumed ideal detector position at 60° in regards to the interaction point (a reasonable finding consistent with previous experiments). Using the spectrum itself to perform a Doppler correction eliminates these kinds of systematic errors arising from difficult to control experimental uncertainties (like the exact detector and target positions). Having multiple line positions and spectral features within the same spectrum is an immediate advantage of using high-resolution, broad range MMC detectors compared to conventional detection methods. Because of an unresolved superposition of the two transitions from the $2s_{1/2}$ and $2p_{1/2}$ states of $\approx 7\,\mathrm{eV}$, the Ly-α_2 lines were excluded from the fit.

Besides K-shell transitions in hydrogen-like xenon, several lines stemming from helium-like xenon ions were

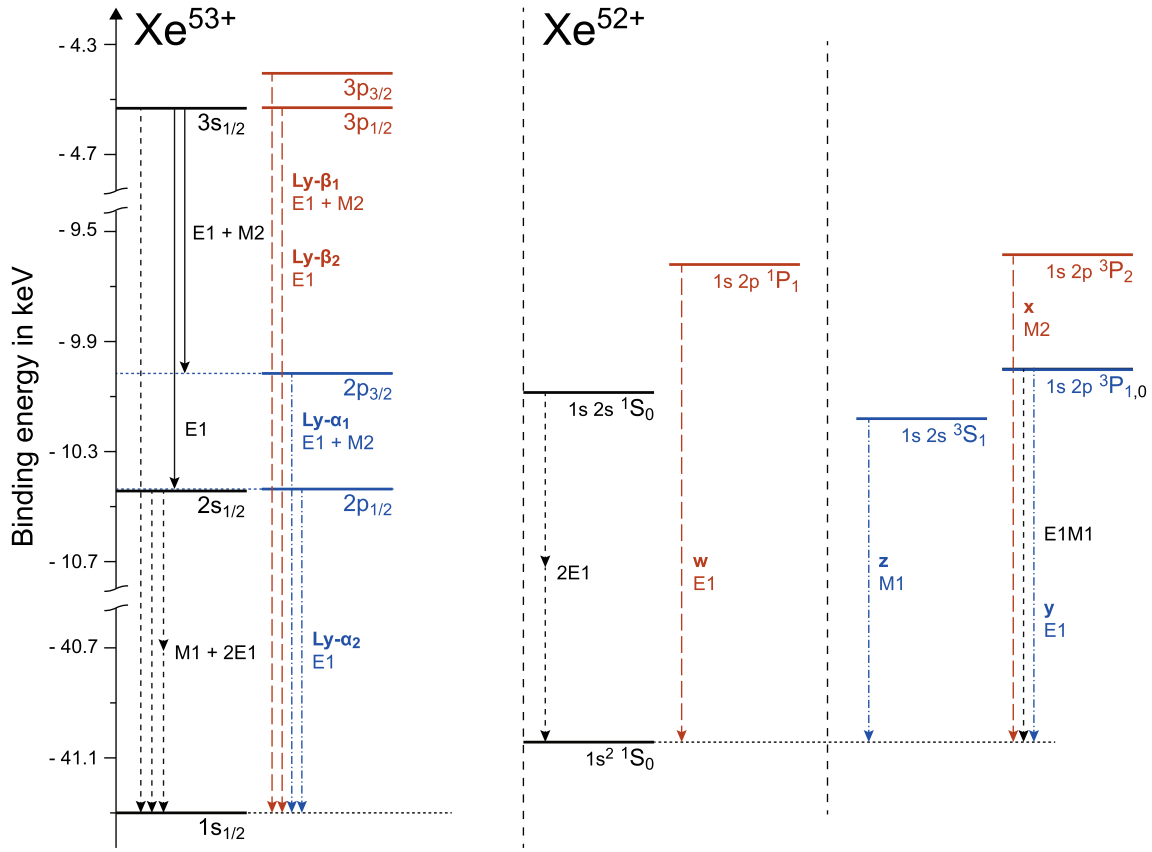

Fig. 2 Displayed are the level schemes for hydrogen (left) and helium-like xenon ions (right). The observed K-α (blue, dash-dot) and K-β (red, long dash) transitions are highlighted. The respective binding energies were taken from our theoretical predictions [17] calculated using the *MDFGME* code (see [18] and refs. there in): It includes finite nuclear size effects (experimental charge radius from [19]), nuclear recoil contributions including relativistic corrections as well as first- and second-order QED corrections. For the two-electron calculations, more details can be found in [20,21]

Table 1 The table contains the measured line positions of the most prominent observed X-ray transitions in hydrogen-like xenon

Transition	E_i [eV]	$E_i - E_f$ [eV]	
Xe^{53+}	Theory	Theory	Experiment emit. system
$2p_{3/2} \rightarrow 1s_{1/2}$	−10,015.94	31,283.92	31,284.00 ± 2.87
$3p_{1/2} \rightarrow 1s_{1/2}$	−4593.26	36,706.61	36,706.28 ± 4.52
$3p_{3/2} \rightarrow 1s_{1/2}$	−4466.24	36,833.63	36,833.79 ± 3.70

The photon energies are given in relation to the moving emitter reference frame and include the statistical uncertainties resulting from fitting errors as well as systematic uncertainties from the Doppler correction. Additionally, the corresponding initial excited state binding energy and transition energy from our theoretical predictions [17] are given

identified as well (see Table 2). This means, that in some collisions two electrons were transferred from the target atoms to the projectiles at once. A comparison between measured line positions with theoretical predictions shows an overall good agreement within the boundaries of statistical and systematic uncertainty. The $1s\ 2p\ ^1P_1 \rightarrow 1s^2\ ^1S_0$ line is overlapped by a second transition from the $1s\ 2p\ ^3P_2$ state and could not be resolved.

3.2.2 K-α satellite peaks

There is no apparent reason to assume that the second electron always has to be captured into the ground state of the helium-like system. Thus, one expects to find K-shell transitions for two electron configurations with the second electron in a higher orbital as well. Both, the Ly-α_1 and Ly-α_2 lines seem to exhibit small satellites on their lower energy edges. The analysis of the Ly-α_1 satellite yields a plateau with a center distance of 123.0 eV in relation to the main peak and a line broadening

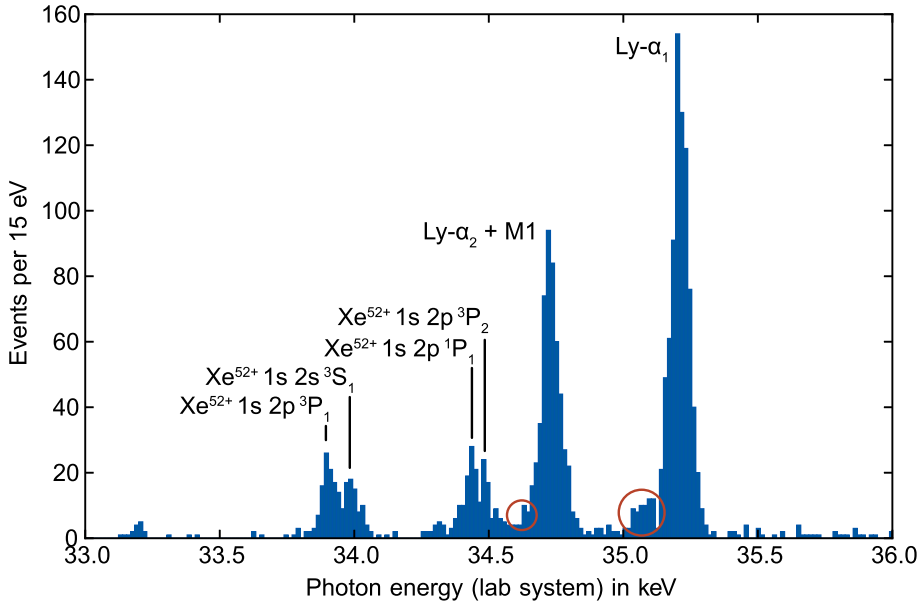

Fig. 3 The spectrum shows spectral details of several recorded Doppler-shifted K-α lines emitted from both hydrogen- and helium-like xenon projectile ions. The satellite features of the Ly-α lines are highlighted by red circles

Table 2 In this table, the measured line positions of K-α transitions in helium-like xenon projectile ions are listed

Transition	ΔE_{exp} [eV]	$\lvert\Delta E_{\mathrm{exp}} - \Delta E_{\mathrm{theo}}\rvert$ [eV]		
Xe52+	emitter sys.	Johnson	Drake	Artemyev
$1s\ 2s\ {}^3\mathrm{S}_1 \rightarrow 1s^2\ {}^1\mathrm{S}_0$	30,124.68 ± 2.85	4.42	3.71	4.46
$1s\ 2p\ {}^3\mathrm{P}_1 \rightarrow 1s^2\ {}^1\mathrm{S}_0$	30,203.50 ± 3.17	2.7	2.08	2.77

The energies are given with respect to the moving emitter's frame of reference and contain uncertainties both from fitting errors and from the used Doppler correction. Furthermore, the table includes the absolute difference between the measured energies and several theoretical predictions from Johnson [26], Drake [27] and Artemyev [28]

to 100 eV. A calculation was performed using FAC [29] exploring all possible transition energies and branching ratios for Ly-α_1-like transitions with an additional electron in the $2p$-orbitals. The second charge in the L-shell partially shields the electric field of the nucleus acting upon the other electron, thus reducing its binding energy. As a result, since the K-shell binding energy is less effected by the L-electron's shielding effect, the overall K-α-transition energy of the system is reduced. In total, two groups of lines are found. Their position coincides with the observed satellites. The transition strength weighted average line energy for the Ly-α_1 satellite yields a distance of 109.4 eV to the main peak and a width of $\sigma = 25$ eV. Taking into account the measured X-ray's line width of 77 eV, the resulting total width of the plateau is expected to be 96.8 eV which fits the observed spectral feature's properties well. Therefore, we attribute these peaks to satellite features of the Ly-α lines. However, due to low statistics an exact determination is not possible. Although the simultaneous transfer of three or more electrons from the target to the projectile ions cannot be ruled out completely, no indication of the occurrence was observed.

3.2.3 Comparison to previous experiment findings

In the past, similar experiments were conducted by other groups measuring K-α-transition energies in different charge states of xenon. For example, a single-pass collision experiment using Xe ions as projectiles on a thin carbon foil was performed at the *LISE* beam line of GANIL, France [2]: The reported transition energies for K-α_1 (31,278 ±10 eV) and $1s\ 2p\ {}^3\mathrm{P}_1 \rightarrow 1s^2\ {}^1\mathrm{S}_0$ (30,209.6 ± 3.5 eV) agree with the results presented in this work. In both experiments, occasionally more than one electron was captured from the target, leading to an unavoidable mixture of transitions from different charge states of Xe ions in the final spectra. However, in comparison to the Ge-based semiconductor detector used at LISE, the higher resolving power of the MMC detector enabled the simultaneous observation of both H-like and He-like transitions as separate lines. This not only eliminates the need to disentangle potentially overlapping transitions during the analysis, but also allows for a more direct comparison of the energies and intensities of these lines.

Another high-resolution measurement of highly char ged Xe ions was performed using a different type of microcalorimeter (Si-thermistor based) detector at an

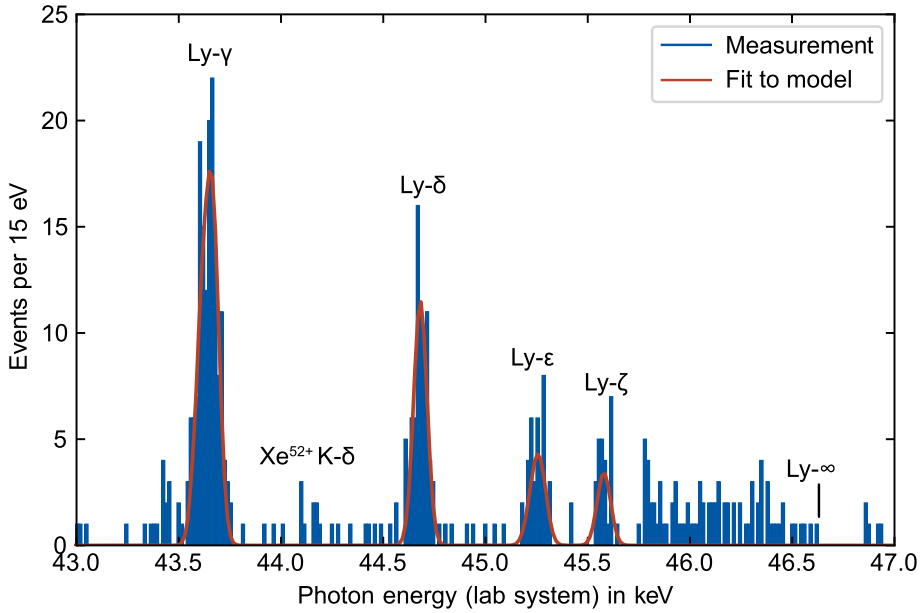

Fig. 4 The spectrum shows details of recorded Doppler-shifted lines stemming from K-shell transitions emitted from both hydrogen- and helium-like xenon projectile ions up the the series limit

electron-beam ion-trap (EBIT) at the Lawrence Livermore National Laboratory, USA [4]: Again, the experimental findings for the K-α_1 (31,284.9 ± 1.8 eV) as well as the y- ($1s\ 2p\ ^3\mathrm{P}_1 \rightarrow 1s^2\ ^1\mathrm{S}_0$, 30,207.1 ± 1.4 eV) and z- ($1s\ 2s\ ^3\mathrm{S}_1 \rightarrow 1s^2\ ^1\mathrm{S}_0$, 30,128.6 ± 1.3 eV) lines of the helium-like system are in good agreement with results of our current work. Though, in principle MMCs are expected to have a higher intrinsic resolution power than semiconductor-based calorimeters [30], the absorber volume of the maXs-200 pixels was optimized for a higher energy range (up to 200 keV compared to 100 keV of the Si thermistor). Because of that, both, the MMC and the semiconductor-based *EBIT calorimeter system* (ECS) used at by Thorn et al. yield a comparable energy resolution of around 35–40 eV (FWHM) in the region of interest around 35 keV. However, despite the similar energy resolutions, a higher precision was achieved at the EBIT. This can be partially explained by the fact that during the ESR measurement fewer events were recorded overall. More importantly though, the line widths of transitions stemming from the fast moving projectile ions were broadened to 77 eV as briefly discussed in Sect. 2.1. This highlights the inherent property of the EBIT measurement of not requiring a Doppler correction or being effected by other relativistic effects compared to the ion–atom collision. However, performing the experiment at an ion storage ring might still be advantageous as a projectile beam of clean isotopes and a well defined charge state is available for the collision. Less overlapping transitions of different charge states are present in the resulting spectrum and even transitions from higher orbitals with quantum numbers $n > 2$ are observable up to the continuum edge as shown in Fig. 4.

3.2.4 1*s*-Lamb shift of hydrogen-like xenon

By definition, the 1*s*-Lamb shift of hydrogen-like xenon amounts to the difference between the real ground state binding energy and the value predicted by Dirac theory for the interaction of a single 1*s*-electron with a point like nucleus (−41,346.80 eV). The resulting value of 46.87 ± 2.78 eV is in excellent agreement with our theoretical prediction (47.094 eV, [17]) and calculations by V. A. Yerokhin (46.920 eV, [31]). Compared to previous experimental results (54 ± 10 eV [2]), a higher accuracy was achieved due to the better energy resolution of the MMC detector in comparison to the Ge detector (reported 270 eV FWHM in the region of interest [2]).

4 Conclusion and outlook

In the present study, the results achieved are strongly affected by the moderate counting statistics. A long distance between the detector and interaction point due to geometrical constraints of the setup and a small detector area because of missing pixels reduced the available solid angle of the observation. Additionally, many of the temperature correction procedures that were developed over the period of subsequent experiment campaigns were not yet available at the time of this experiment, thus further reducing the final energy resolution. Nevertheless, quite accurate results for the transition energies could be obtained. Overall, the findings are in a good agreement with both theoretical predictions as well as previous experimental findings. Taking into account that this was one of the first experiments utilizing a maXs-series detector for atomic physics measurements at an ion storage ring, it proves the feasibility

of future beam times exploiting the excellent performance of these detectors. In particular, the recorded spectrum did contain almost no background events even without applying time coincidence filtering. Systematic uncertainties stemming from difficult to predict experiment setup parameters like the position of the gas-jet within the target chamber or even the slight shift of the detector position due to thermal contraction during the cool-down phase could be mostly eliminated by using multiple highly resolved lines within the same recorded spectrum.

Meanwhile, detectors of the maXs-series have been improved significantly. The newly designed maXs-30 [8] and -100 [9] detectors consist of 8×8 pixels with an increased active detection area and correct several issues that occurred over time. For example, temperature sensitive pixels have been added to allow for an intrinsic temperature correction of the obtained spectra. Accompanying the changes to the hardware, calibration and measurement procedures have been updated as well. Furthermore, the maXs-detector family will be integrated into the heterogeneous detector environment of the FAIR complex which is currently being built [32]. This allows for them to be used, e.g., with particle detectors to perform coincidence measurements and further improve their accuracy by suppressing background events. This could help with a better identification of small spectral features like the discussed satellite structures found near the Ly-α lines. Such an application has been recently demonstrated in the first high-resolution measurement of K-α transitions in He-like uranium U^{90+} at the electron cooler of the *CRYRING@ESR* low energy ion storage ring of FAIR [33]. Further experiments utilizing MMC detectors for high-precision atomic physics experiments involving highly charged ions in storage rings like CRYRING@ESR are already planned.

Acknowledgements We thank all participating members of the research division for atomic, quantum and fundamental research of GSI and of the KIP that helped with the experiment setup and execution. This work was created within the SPARC collaboration and was supported in part by the ExtreMe Matter Institute EMMI at the GSI Helmholtzzentrum für Schwerionenforschung, Darmstadt.

Author contributions

Analysis software, data analysis and presentation of the results: MOH; Design, manufacturing and operation of microcalorimeter detectors: DH, MKe, JG, CS, MKr, AF and all other participating members of the group of CE; Experiment at ESR: P-MH, TG, AG, ST, US and all participating members of GSI; Theory: PI; Supervision, project administration and idea: Th.S. All authors have read and agreed to the published version of the manuscript.

Funding Open Access funding enabled and organized by Projekt DEAL. We acknowledge financial support by the European Union and the federal state of Thuringia via Thüringer Aufbaubank within the ESF Project (2018 FGR 0080). The work was supported by the BMBF Grant 05P12VHFA5.

Data Availability Statement This manuscript has no associated data or the data will not be deposited. The data that support the findings of this study are available upon reasonable request from the authors.

Declarations

Conflict of interest The authors declare no conflict of interest. The funders had no role in the design of the study; in the collection, analyses, or interpretation of data; in the writing of the manuscript; or in the decision to publish the results.

Ethics approval Not applicable.

Consent to participate Not applicable.

Consent for publication Not applicable.

Code availability Not applicable.

References

1. P. Indelicato, Topical Review: QED tests with highly-charged ions. J. Phys. B **52**, 232001 (2019). https://doi.org/10.1088/1361-6455/ab42c9
2. J.P. Briand, P. Indelicato, A. Simionovici, V. San Vicente, D. Liesen, D. Dietrich, Spectroscopic study of hydrogenlike and heliumlike xenon ions. Europhys. Lett. **9**(3), 225–230 (1989). https://doi.org/10.1209/0295-5075/9/3/007
3. K. Widmann, P. Beiersdorfer, G.V. Brown, J.R.C. López-Urrutia, A.L. Osterheld, K.J. Reed, J.H. Scofield, S.B. Utter, High-resolution measurements of the k-shell spectral lines of hydrogenlike and heliumlike xenon. AIP Conf. Proc. **506**(1), 444–466 (2000). https://doi.org/10.1063/1.1302773
4. D.B. Thorn, M.F. Gu, G.V. Brown, P. Beiersdorfer, F.S. Porter, C.A. Kilbourne, R.L. Kelley, Precision measurement of the K-shell spectrum from highly

charged xenon with an array of X-ray calorimeters. Phys. Rev. Lett. **103**(16), 0163001 (2009). https://doi.org/10.1103/PhysRevLett.103.163001
5. J. Eichler, T. Stöhlker, Radiative electron capture in relativistic ion-atom collisions and the photoelectric effect in hydrogen-like high-z systems. Phys. Rep. **439**(1), 1–99 (2007). https://doi.org/10.1016/j.physrep.2006.11.003
6. A. Fleischmann, Magnetische Mikrokalorimeter: Hochauflösende Röntgenspektroskopie Mit Energiedispersiven Detektoren. PhD Thesis, Ruprecht-Karls-Universität Heidelberg (2003). https://www.kip.uni-heidelberg.de/Veroeffentlichungen/download.php/4385/ps/fleischmann-diss.pdf
7. C. Pies, maXs-200: Entwicklung Und Charakterisierung Eines Röntgendetektors Basierend Auf Magnetischen Kalorimetern Für Die Hochauflösende Spektroskopie Hochgeladener Ionen. PhD Thesis, Ruprecht-Karls-Universität Heidelberg (2012). https://www.kip.uni-heidelberg.de/Veroeffentlichungen/download.php/5430/temp/2731.pdf
8. D. Hengstler, Development and Characterization of Two-Dimensional Metallic Magnetic Calorimeter Arrays for the High-Resolution X-ray Spectroscopy. PhD Thesis, Ruprecht-Karls-Universität Heidelberg (2017). https://archiv.ub.uni-heidelberg.de/volltextserver/23815/1/Dissertation.pdf
9. J. Geist, Bestimmung Der Isomerenergie von 229Th Mit Dem Hochauflösenden Mikrokalorimeter-Array maXs30. PhD Thesis, Ruprecht-Karls-Universität Heidelberg (2020). http://archiv.ub.uni-heidelberg.de/volltextserver/id/eprint/27683
10. C. Pies, S. Schäfer, S. Heuser, S. Kempf, A. Pabinger, J.-P. Porst, P. Ranitsch, N. Foerster, D. Hengstler, A. Kampkötter, T. Wolf, L. Gastaldo, A. Fleischmann, C. Enss, maXs: microcalorimeter arrays for high-resolution X-ray spectroscopy at GSI/FAIR. J. Low Temp. Phys. **167**(3–4), 269–279 (2012). https://doi.org/10.1007/s10909-012-0557-z
11. A. Fleischmann, C. Enss, G.M. Seidel, Metallic magnetic calorimeters, in *Cryogenic Particle Detection. Topics in Applied Physics*. ed. by C. Enss (Springer, Berlin, 2005), pp.151–216. https://doi.org/10.1007/10933596_4
12. D. Hengstler, M. Keller, C. Schötz, J. Geist, M. Krantz, S. Kempf, L. Gastaldo, A. Fleischmann, T. Gassner, G. Weber, R. Märtin, T. Stöhlker, C. Enss, Towards FAIR: first measurements of metallic magnetic calorimeters for high-resolution X-ray spectroscopy at GSI. Phys. Scr. **T166**, 014054 (2015). https://doi.org/10.1088/0031-8949/2015/T166/014054
13. P.-M. Hillenbrand, S. Hagmann, Y.S. Kozhedub, E.P. Benis, C. Brandau, R.J. Chen, D. Dmytriiev, O. Forstner, J. Glorius, R.E. Grisenti, A. Gumberidze, M. Lestinsky, Y.A. Litvinov, E.B. Menz, T. Morgenroth, S. Nanos, N. Petridis, P. Pfäfflein, H. Rothard, M.S. Sanjari, R.S. Sidhu, U. Spillmann, S. Trotsenko, I.I. Tupitsyn, L. Varga, T. Stöhlker, Single and double K-shell vacancy production in slow $Xe^{54+,53+}$-Xe collisions. Phys. Rev. A **105**(2), 022810 (2022). https://doi.org/10.1103/PhysRevA.105.022810
14. P.-M. Hillenbrand, K.N. Lyashchenko, S. Hagmann, O.Y. Andreev, D. Banaś, E.P. Benis, A.I. Bondarev, C. Brandau, E. De Filippo, O. Forstner, J. Glorius, R.E. Grisenti, A. Gumberidze, D.L. Guo, M.O. Herdrich, M. Lestinsky, Y.A. Litvinov, E.V. Pagano, N. Petridis, M.S. Sanjari, D. Schury, U. Spillmann, S. Trotsenko, M. Vockert, A.B. Voitkiv, G. Weber, T. Stöhlker, Electron-loss-to-continuum cusp in collisions of U^{89+} with N_2 and Xe. Phys. Rev. A **104**(1), 012809 (2021). https://doi.org/10.1103/PhysRevA.104.012809
15. F.M. Kröger, G. Weber, M.O. Herdrich, J. Glorius, C. Langer, Z. Slavkovská, L. Bott, C. Brandau, B. Brückner, K. Blaum, X. Chen, S. Dababneh, T. Davinson, P. Erbacher, S. Fiebiger, T. Gaßner, K. Göbel, M. Groothuis, A. Gumberidze, G. Gyürky, S. Hagmann, C. Hahn, M. Heil, R. Hess, R. Hensch, P. Hillmann, P.-M. Hillenbrand, O. Hinrichs, B. Jurado, T. Kausch, A. Khodaparast, T. Kisselbach, N. Klapper, C. Kozhuharov, D. Kurtulgil, G. Lane, C. Lederer-Woods, M. Lestinsky, S. Litvinov, Y.A. Litvinov, B. Löher, F. Nolden, N. Petridis, U. Popp, M. Reed, R. Reifarth, M.S. Sanjari, H. Simon, U. Spillmann, M. Steck, J. Stumm, T. Szücs, T.T. Nguyen, A. Taremi Zadeh, B. Thomas, S.Y. Torilov, H. Törnqvist, C. Trageser, S. Trotsenko, M. Volknandt, M. Weigand, C. Wolf, P.J. Woods, V.P. Shevelko, I.Y. Tolstikhina, T. Stöhlker, Electron capture of Xe^{54+} in collisions with H_2 molecules in the energy range between 5.5 and 30.9 MeV/u. Phys. Rev. A **102**(4), 042825 (2020). https://doi.org/10.1103/PhysRevA.102.042825
16. M. Keller, *Erster Test eines metallischen magnetischen Kalorimeters am Experimentellen Speicherring ESR der GSI* (Ruprecht-Karls-Universität Heidelberg, Bachelorarbeit, 2014)
17. P. Indelicato, unpublished (2019)
18. P. Indelicato, Mcdfgme, a Multiconfiguration Dirac Fock and General Matrix Elements Program (Release 2022v3) (2022). http://www.lkb.upmc.fr/metrologysimplesystems/mdfgme-a-general-purpose-multiconfiguration-dirac-foc-program/
19. I. Angeli, K.P. Marinova, Table of experimental nuclear ground state charge radii: an update. At. Data Nucl. Data Tables **99**(1), 69 (2013). https://doi.org/10.1016/j.adt.2011.12.006
20. O. Gorceix, P. Indelicato, J.P. Desclaux, MCDF studies of two electron ions I: electron–electron interaction. J. Phys. B **20**(4), 639 (1987). https://doi.org/10.1088/0022-3700/20/4/006
21. P. Indelicato, O. Gorceix, J.P. Desclaux, MCDF studies of two electron ions II: radiative corrections and comparison with experiment. J. Phys. B **20**(4), 651 (1987)
22. A.A. Kotov, D.A. Glazov, V.M. Shabaev, G. Plunien, One-electron energy spectra of heavy highly charged quasimolecules: finite-basis-set approach. Atoms **9**(3), 044 (2021). https://doi.org/10.3390/atoms9030044
23. T. Gassner, High Precision X-Ray Spectroscopy of Highly Charged Heavy Ions. PhD Thesis, Friedrich-Schiller-Universität Jena (2016). https://www.db-thueringen.de/servlets/MCRFileNodeServlet/dbt_derivate_00037490/Gassner_Thesis_final_PDFA-1b.pdf
24. R.D. Deslattes, E.G. Kessler Jr., P. Indelicato, L. Billy, E. Lindroth, J. Anton, X-ray transition energies: new approach to a comprehensive evaluation. Rev. Mod. Phys. **75**(1), 35 (2003). https://doi.org/10.1103/RevModPhys.75.35

25. C. Scheidenberger, T. Stöhlker, W.E. Meyerhof, H. Geissel, P.H. Mokler, B. Blank, Charge states of relativistic heavy ions in matter. Nucl. Instrum. Methods Phys. Res. Sect. B **142**(4), 441–462 (1998). https://doi.org/10.1016/S0168-583X(98)00244-4
26. W.R. Johnson, D.R. Plante, J. Sapirstein, Relativistic calculations of transition amplitudes in the helium isoelectronic sequence, in *Advances in Atomic, Molecular, and Optical Physics*, vol. 35, ed. by B. Bederson, H. Walther (Elsevier, Amsterdam, 1995), pp.255–329. https://doi.org/10.1016/S1049-250X(08)60165-2
27. G.W. Drake, Theoretical energies for the n = 1 and 2 states of the helium isoelectronic sequence up to Z = 100. Can. J. Phys. **66**(7), 586–611 (1988). https://doi.org/10.1139/p88-100
28. A.N. Artemyev, V.M. Shabaev, V.A. Yerokhin, G. Plunien, G. Soff, QED calculation of the n = 1 and n = 2 energy levels in He-like ions. Phys. Rev. A **71**(6), 062104 (2005). https://doi.org/10.1103/PhysRevA.71.062104
29. M.F. Gu, The flexible atomic code. Can. J. Phys. **86**(5), 675–689 (2008). https://doi.org/10.1139/p07-197
30. C. Enss, *Cryogenic Particle Detection. Topics in Applied Physics* (Springer, Berlin, 2005). https://doi.org/10.1007/b12169
31. V.A. Yerokhin, V.M. Shabaev, Lamb shift of n = 1 and n = 2 states of hydrogen-like atoms, 1 ≤ Z ≤ 110. J. Phys. Chem. Ref. Data **44**(3), 033103 (2015). https://doi.org/10.1063/1.4927487
32. M. Durante, P. Indelicato, B. Jonson, V. Koch, K. Langanke, U.-G. Meißner, E. Nappi, T. Nilsson, T. Stöhlker, E. Widmann, M. Wiescher, All the fun of the fair: fundamental physics at the facility for antiproton and ion research. Phys. Scr. **94**(3), 033001 (2019). https://doi.org/10.1088/1402-4896/aaf93f
33. P. Pfäfflein, S. Allgeier, S. Bernitt, A. Fleischmann, M. Friedrich, C. Hahn, D. Hengstler, M.O. Herdrich, A. Kalinin, F.M. Kröger, P. Kuntz, M. Lestinsky, B. Löher, E.B. Menz, T. Over, U. Spillmann, G. Weber, B. Zhu, C. Enss, T. Stöhlker, Integration of maXs-type microcalorimeter detectors for high-resolution X-ray spectroscopy into the experimental environment at the CRYRING@ESR electron cooler. Phys. Scr. **97**(11), 0114005 (2022). https://doi.org/10.1088/1402-4896/ac93be